Coastal Engineering xxx (2010) xxx–xxx

Contents lists available at ScienceDirect

Coastal Engineering

journal homepage: www.elsevier.com/locate/coastaleng

Effects of wave–current interaction on the current profile

Maitane Olabarrieta *, Raul Medina, Sonia Castanedo

Environmental Hydraulic Institute, IH Cantabria, Universidad de Cantabria, E.T.S.I. Caminos, Canales y Puertos, Avd. Los Castros s/n., 39005 Santander, Spain

ARTICLE INFO

Article history:
Received 9 October 2008
Received in revised form 2 February 2010
Accepted 11 February 2010
Available online xxxx

Keywords:
Wave–current interaction
Boundary layers
Apparent bed roughness
Reynolds stresses
Turbulence

ABSTRACT

Wave–current laboratory experiments have shown that the logarithmic current profile observed in pure current flows is modified due to the presence of waves. When waves propagate opposite the current, an increase in the current intensity is achieved near the mean water level, while a reduction is obtained for following waves and currents. With the aim of analyzing these nonlinear effects along the whole water column, an Eulerian wave–current model is presented. In contrast to previously presented wave–current models, the present is able to include the variation of the free surface elevation due to the wave motion and the effect of a non hydrostatic pressure field. Therefore it does not restrict its application to waves in shallow waters. Moreover, the model is able to simulate all the possible angles between waves and currents.
Several available experimental steady current profiles in combined flows, covering different current regimes, angles between waves and currents and different bed roughness, are considered in the model validation. In general, a good agreement between the measured and the computed profiles is obtained. The model is able to predict the differences observed between following and opposing waves, not only near the mean water level but also near the bottom. As shown in the experiments, the model reproduces the reduction of the apparent bed roughness observed in following cases with smooth bed and the increase in rough bed conditions. In order to have a better understanding of the wave–current interaction process, the model is applied to different combined flow cases. The results obtained are shown and discussed in the present paper.

1. Introduction

It is well known that in coastal regions, such as estuaries and beaches, waves and currents coexist simultaneously, being the most important processes controlling the hydrodynamic behavior. However, the non-linear interaction between these two processes is still not well understood and, as several studies (Moon, 2005; Bolaños-Sanchez et al., 2005; Kang and Iorio, 2006, among others) have demonstrated, can play an important role in wave dynamics, in hydrodynamics and also in sediment transport processes.

In the last decades, important efforts have been carried by the scientific community with the purpose of analyzing the aforementioned non linear interaction. Studies based on laboratory experiments (Kemp and Simons, 1982, 1983; Visser, 1986; Klopman, 1994, 1997; Umeyama, 2005; Musumeci et al., 2006; Simons et al., 1996 among others) have shown that when waves and currents coexist, the steady current profile loses the logarithmic shape observed in pure current conditions. Experimental investigations performed by Kemp and Simons (1982) showed that mean velocities near a smooth bed are increased by the presence of waves, whereas near a rough bed they are reduced. When waves propagate opposite the current, a reduction of the current intensity near the bed is also observed. Musumeci et al. (2006) showed that when the bed is smooth, an increase of the near bottom velocities occurs when waves are perpendicular to the current. The opposite happens when the bottom is rough. Moreover, measured current profiles suggest that wave–current interaction effects are not restricted to the near bottom region, but apply to the entire water column (Kemp and Simons, 1982, 1983; Klopman, 1994; Umeyama, 2005). These effects are greatly dependent on wave and current propagation direction. While for following and perpendicular cases a reduction of the current intensity is observed in the region below the wave trough, the contrary occurs for opposing waves and currents. As stated by Kemp and Simons (1983) steady current profile variations also depend on wave amplitude and on water depth. It is worth noting that these laboratory experiments showed that the apparent bed roughness variation does not always correspond to an increment. In some cases, usually for following and perpendicular waves and currents, a decrease occurs (Kemp and Simons (1982), Musumeci et al. (2006)).

Wave–current interaction has also been analyzed by analytical and numerical models. Analytical models (Kajiura, 1968; Grant and Madsen, 1979; Fredsøe, 1984; Nielsen, 1986; O'Connor and Yoo, 1988; Huang and Mei, 2003) consider a 1D wave–current interaction problem, in which the vertical structure of the combined flow is solved, assuming a simple vertical turbulence structure.

In addition to the analytical studies, different numerical models have been developed to describe the bottom boundary layer flow under waves plus currents (Holmedal et al., 2003). These models can be

* Corresponding author. Tel.: +34 942202852; fax: +34 942202860.
E-mail addresses: olabarrim@unican.es (M. Olabarrieta), medinar@unican.es (R. Medina), castanedos@unican.es (S. Castanedo).

0378-3839/$ – see front matter © 2010 Elsevier B.V. All rights reserved.
doi:10.1016/j.coastaleng.2010.02.003

classified according to the reference frame used to solve the flow structure: The classical Eulerian models and the more recent Lagrangian ones. The Eulerian models have been widely used in wave–current interaction analysis. The considered vertical turbulence closure model is the main difference between the models. Christoffersen and Jonsson (1985) used the time invariant eddy viscosity, while Myrhaug and Slaattelid (1990) applied a similarity model. Bakker and van Doorn (1978) used the Prandlt mixing length model to calculate the velocity profiles under combined flows. Davies et al. (1988) used a one-equation turbulent energy closure to calculate the flow over the entire water column, assuming the streamlines to be parallel. Another approach was taken by Huynh-Thanh and Temperville (1991) and Harris (1997), using a two-equation turbulence closure to solve the bottom boundary layer under sinusoidal waves plus currents. Sheng (1983) considered a Reynolds stress equation model. As in the analytical studies, in all the aforementioned Eulerian numerical models, only the vertical dimension has been considered, neglecting the effects of the advective terms in momentum conservation equations.

Nielsen and You (1996) presented a two dimensional wave–current interaction model for weak current conditions. Kim et al. (2001), based on the model developed by Davies et al. (1988), but applying a mixing length hypothesis, presented a numerical model in which the vertical advective terms were included. In this model it was also possible to simulate perpendicular and oblique wave–current conditions. They concluded that the inclusion of the vertical advective terms is essential to describe the differences observed between following and opposing combined flows. A noteworthy fact is that most of these models consider a rigid lid condition for the free surface or are applied only to the bottom boundary layer. That is why they are not able to solve the flow over the entire water column, including the zone between the trough and the crest of the wave. Moreover, the hypothesis of shallow water is usually assumed, and therefore, no pressure vertical variations are considered.

On the other hand, 2DV Lagrangian models are based on the Generalized Lagrangian Mean (GLM) approach (Dingemans et al. (1996), Groeneweg and Klopman (1998), Groeneweg and Battjes (2003)). As described by Groeneweg and Battjes (2003), the GLM description enables splitting the mean and oscillating motion over the entire water depth. The GLM equations provide a very general Lagrangian-mean description on the feedback of oscillatory disturbances upon the mean state. These equations depict a Lagrangian-mean velocity field about which fluctuating particle motions have zero mean, when a temporal, spatial, ensemble or other averaging process is applied.

Although GLM models are capable of solving the flow structure over the entire water column, most studies on wave–current interaction have focused on the processes taking place within the boundary layer, giving less attention to those observed over the entire water column. Therefore, the aim of this paper is to analyze the effect of wave–current interaction over the whole current profile considering following, opposing and perpendicular wave–current conditions. With the aforementioned scope, and based on the model presented by Kim et al. (2001), a numerical model has been developed. In contrast to Kim et al. (2001), in this model all the advective terms are considered and its application is not restricted to shallow water waves. Moreover, the model is able to simulate those effects induced by the wave finite amplitude which creates depth variations due to the oscillatory motion. This effect has not been analyzed in detail so far. However, the model does not consider the non-linearity of the surface waves in the sense that waves are simulated as sinusoidal waves. Note that the model does not consider the effect of Craik–Leibovich vortex forces nor the wave decay process.

Most of the models able to solve combined-flows, both Eulerian and Lagrangian ones, have been tested with few laboratory data, usually with the measurements carried out by Klopman (1994, 1997). Furthermore, few numerical models have been used to simulate wave and current perpendicular situations. Therefore, the second purpose of this paper is to test the numerical model, covering the widest range of situations in which this interaction can occur. The last purpose of the paper is to use the developed numerical model in order to investigate how the wave–current interaction affects the mean steady current profile.

The paper is organized as follows. In Section 2 the basic equations, the turbulence closure and the numerical treatment are outlined. In order to validate the model and demonstrate its performance, a comparison between measured current profiles and the simulated ones is presented in Section 3. The increase of the apparent bed roughness is calculated using the experimental current profiles, and in Section 4 the real variation of this parameter is compared with the one predicted by the present model. In Section 5, the effects induced in the steady current profile by changes in the wave height and in the wave period are described. This analysis considers different angles of incidence between waves and currents. Finally, in Section 6, the derived conclusions are outlined.

2. Model description

The vertical structure of the flow under waves and currents can be derived from the three dimensional Navier Stokes equations and the continuity equation. In this paper, the propagation of waves and currents over a flat bed is considered. The horizontal coordinates at the bed are given as (x,y), while the vertical coordinate z gives the distance from the bed. The bed is fixed at $z=z_0$, being z_0 the physical bed roughness. Waves propagating in shallow or intermediate water depths are considered, and therefore, the horizontal components of the shear stresses can be neglected compared to the vertical ones. Following Kim et al. (2001) the Cartesian x-axis is selected to follow the wave propagation direction. This makes the derivatives of the velocity in the y axis equal to zero, simplifying the governing equations to the following expressions:

$$\frac{\partial u}{\partial x} + \frac{\partial w}{\partial z} = 0 \tag{1}$$

$$\frac{\partial u}{\partial t} + u\frac{\partial u}{\partial x} + w\frac{\partial u}{\partial z} = -\frac{1}{\rho}\frac{\partial P_T}{\partial x} + \frac{\partial}{\partial z}[\tau_{xz}] \tag{2}$$

$$\frac{\partial v}{\partial t} + u\frac{\partial v}{\partial x} + w\frac{\partial v}{\partial z} = -\frac{1}{\rho}\frac{\partial P_T}{\partial y} + \frac{\partial}{\partial z}\left[\tau_{yz}\right] \tag{3}$$

$$\frac{\partial w}{\partial t} + \frac{1}{\rho}\frac{\partial P_T}{\partial z} = -g \tag{4}$$

where u, v and w = longitudinal, lateral, and vertical orbital velocities, respectively: t = time; x, y and z = longitudinal, lateral and vertical Cartesian coordinates, respectively; ρ = water density; P_T = total pressure; τ_{xz} and τ_{yz} = turbulent shear stresses on the x, z plane and y, z plane, respectively; g = gravitational acceleration.

Soulsby et al. (1993) suggested that, in order to accurately describe the wave boundary layer behavior, the dependency of the eddy viscosity with time must be considered. In this paper the Boussinesq approach is assumed. This considers that, in analogy to the molecular movements, shear stresses in a turbulent flow are proportional to a turbulent eddy viscosity and to the velocity field vertical gradient. The equations that relate the aforementioned parameters are the following:

$$\rho\tau_{xz} = \nu_{V,wc}\frac{\partial u}{\partial z};\ \rho\tau_{yz} = \nu_{V,wc}\frac{\partial v}{\partial z} \tag{5}$$

where ν_{wc} represents the vertical eddy viscosity for wave–current flows.

For simplicity, the vertical eddy viscosity closure model is based on the Prandlt mixing length theory, and given by the following expression:

$$\nu_{wc} = l^2 \sqrt{\left(\frac{\partial u}{\partial z}\right)^2 + \left(\frac{\partial v}{\partial z}\right)^2} \tag{6}$$

where l represents the mixing length.

Following Bakker and van Doorn (1978) and Kim et al. (2001), the length scale is assumed to increase with the distance from the bed. Nezu and Rodi (1986), based on experimental measurements made with stationary currents, concluded that the length scale tends to zero near the water surface. Thus, a reduction factor for the length scale is included to take into account this tendency. The equation that includes this linear increase of the mixing length and its reduction near the free surface is given by the following expression:

$$l = \kappa z \sqrt{1 - \frac{z}{h + \tilde{\eta}}} \tag{7}$$

where κ = von Karman constant (=0.4); $\tilde{\eta}$ = sea surface elevation; h = mean water depth. In Fig. 1, the dependency of the length scale with the dimensionless water depth is depicted.

In order to numerically solve expressions (1–4) some considerations about the total pressure term must be taken into account. For a combined wave–current flow, this can be split into two parts, the pressure term that forces the stationary current and another pressure term resulting from the oscillatory motion. This means that the total pressure term is composed by both a stationary and an oscillating term:

$$P_T = p_w + p_c \tag{8}$$

where p_w = oscillatory pressure term; p_c = stationary pressure term.

For nearly horizontal steady flows, the current pressure field is hydrostatic, whereas the wave pressure field includes a hydrostatic and a possible dynamic contribution. In the present numerical model, to calculate the wave pressure field and its dependency with the water depth, the method proposed by Uittenbogaard (2000) is applied. This method assumes that the pressure field is sinusoidal, both in time and in space, its amplitude being dependent on the water depth:

$$p_w = p(z)\cos(-w_a t + k_w x) \tag{9}$$

where $p(z)$ = amplitude of the oscillatory pressure term; w_a = wave absolute frequency; k_w = wave number. The wave absolute frequency and the wave number in wave–current combined flows are related by the dispersion relation that takes into account the Doppler effect:

$$\left(w_a - \frac{2\pi}{L} U\cos(\phi)\right)^2 = g\frac{2\pi}{L}\tanh\left(\frac{2\pi}{L}h\right) \tag{10}$$

where L represents the wave length, ϕ stands for the angle of propagation between waves and currents and U represents the wave period and water depth averaged mean current velocity. The wave length L and the wave number are related by the following expression:

$$L = \frac{2\pi}{k_w} \tag{11}$$

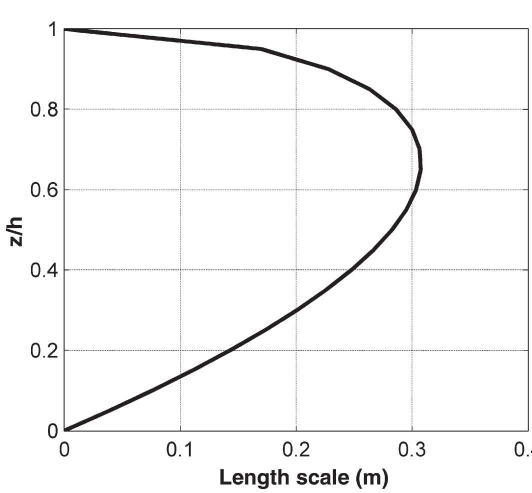

Fig. 1. Mixing length scale dependency with total water depth. In the lower part of the water column the mixing length increases linearly while a reduction is achieved near the free surface.

The pressure amplitude is obtained solving the Rayleigh equation of Hydrodynamic Stability Theory or the inviscid form of the Orr–Sommerfeld equation (Uittenbogaard, 2000):

$$\frac{d^2p}{dz^2} + 2B\frac{dp}{dz} - |k_w|^2 p = 0 \tag{12}$$

where:

$$B = \frac{1}{\Omega(z)} \frac{\partial \overline{U}(z) k_w}{\partial z} \tag{13}$$

$$\Omega(z) = w_r - k_w \overline{U}(z)\cos(\phi) \tag{14}$$

$\overline{U}(z)$ represents the current mean velocity over a wave period. $\Omega(z)$ stands for the depth varying absolute frequency and depends on the current profile, on the relative wave frequency and on the wave number. The vertical integration of this parameter represents the term the absolute wave frequency w_a, defined in Eq. (10).

With regard to the oscillatory motion, like in linear wave theory, a sinusoidal wave is considered. The following expression defines free surface elevation for a sinusoidal wave motion:

$$\tilde{\eta} = \frac{H}{2}\cos(-w_a t + k_w x) \tag{15}$$

In order to include the variation of the free surface level, and at the same time increase the resolution near the bed, a vertical coordinate transformation is done: the z coordinate is transformed into an α coordinate system using the following relation:

$$\alpha = \left(\frac{z - z_0}{h + \tilde{\eta} - z_0}\right)^{1/q} \tag{16}$$

where q is a form coefficient. This transformation allows having higher resolution near the bed (α = 0) and also a time unchanging grid that follows the form of the free surface (α = 1). Therefore a rigid lid condition does not have to be assumed. In Fig. 2 the considered grid transformation is depicted.

Appling this coordinate transformation, the following final governing equations are derived:

Continuity equation

$$\frac{\partial u}{\partial x} + F\frac{\partial w}{\partial \alpha} = 0 \tag{17}$$

where:

$$F = \frac{\partial \alpha}{\partial z} = \frac{1}{q}\frac{1}{(h + \tilde{\eta} - z_0)}\alpha^{(1-q)} \tag{18}$$

Please cite this article as: Olabarrieta, M., et al., Effects of wave–current interaction on the current profile, Coast. Eng. (2010), doi:10.1016/j.coastaleng.2010.02.003

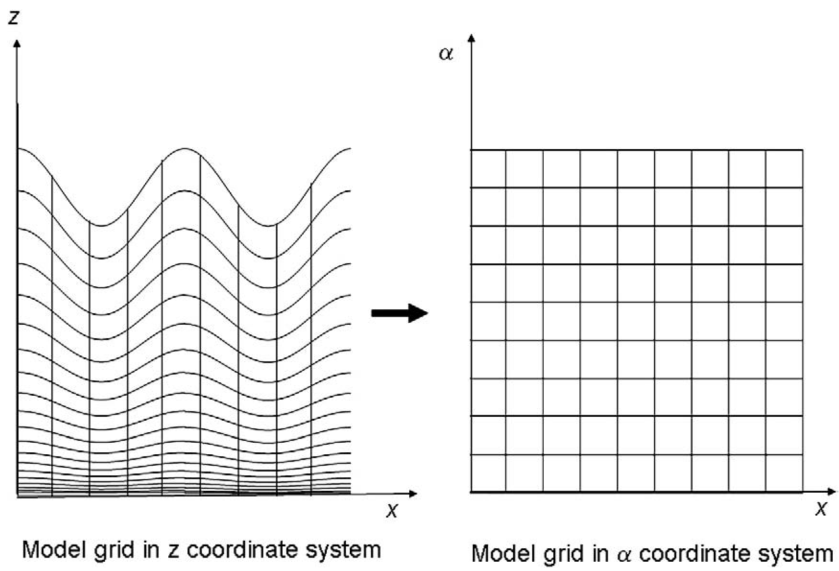

Fig. 2. Transformation from a z vertical coordinate system to an α coordinate system. This transformation allows having higher resolution near the bed and also a time unchanging grid that follows the form of the free surface.

Momentum conservation equations

$$\frac{\partial u}{\partial t} = -u\frac{\partial u}{\partial x} - wF\frac{\partial u}{\partial \alpha} - \frac{1}{\rho}\frac{\partial p}{\partial x} + \frac{1}{\rho}F\frac{\partial \tau'_{xz}}{\partial \alpha} \tag{19}$$

$$\frac{\partial v}{\partial t} = -u\frac{\partial v}{\partial x} - wF\frac{\partial v}{\partial \alpha} - \frac{1}{\rho}\frac{\partial p}{\partial y} + \frac{1}{\rho}F\frac{\partial \tau'_{yz}}{\partial \alpha} \tag{20}$$

where:

$$\tau'_{xz} = \rho F \nu_{V,wc}\frac{\partial u}{\partial \alpha} \tag{21}$$

$$\tau'_{yz} = \rho F \nu_{V,wc}\frac{\partial v}{\partial \alpha} \tag{22}$$

$$\nu_{V,wc} = l^2\sqrt{\left(F\frac{\partial u}{\partial \alpha}\right)^2 + \left(F\frac{\partial v}{\partial \alpha}\right)^2} \tag{23}$$

$$l = \kappa\left[\alpha^q(h+\tilde{\eta}-z_0)+z_0\right]\quad\sqrt{1-\frac{\left[\alpha^q(h+\tilde{\eta}-z_0)+z_0\right]}{h+\tilde{\eta}}} \tag{24}$$

Rayleigh equation

$$F^2\frac{d^2p}{d\alpha^2} + 2BF\frac{dp}{d\alpha} - |k_w|^2 p = 0 \tag{25}$$

where:

$$B = \frac{1}{\Omega(\alpha)}F\frac{\partial \overline{U}(\alpha)k_w}{\partial \alpha} \tag{26}$$

$$\Omega(\alpha) = w_r - k_w\overline{U}(\alpha) \tag{27}$$

In order to solve the governing equations, different boundary conditions have to be applied. In the present model a Dirichlet boundary condition for the vertical and horizontal flow components is applied at the bottom.

$$\begin{aligned} w = 0 \quad \text{in} \quad \alpha = 0 \\ u = 0 \quad \text{in} \quad \alpha = 0 \end{aligned} \tag{28}$$

A Newman boundary condition for the vertical gradient of the vertical shear stresses has been considered in the free surface and near the bed.

$$\nu_{V,wc}\frac{\partial \tau}{\partial \alpha} = 0 \quad \text{in} \quad \alpha = 0 \tag{29}$$

$$\nu_{V,wc}\frac{\partial \tau}{\partial \alpha} = 0 \quad \text{in} \quad \alpha = 1 \tag{30}$$

To solve the Rayleigh equation, the following boundary conditions are applied:

$$(p)_{\alpha=1} = \rho g\tilde{\eta} \tag{31}$$

$$(p)_{\alpha=0} = \rho g\left(\frac{1}{\cosh kh}\right)\tilde{\eta} \tag{32}$$

Moreover, a periodicity condition is imposed over a wavelength. This is determined by the dispersion relation that takes into account the Doppler effect. Note that by imposing a periodicity condition, no wave decay or dissipation is considered by the current numerical model. The numerical model is based on a leap-frog numerical scheme, and for its numerical stability the Courant–Friedrichs–Lewy (CFL) criterion and the stability criterion of Haney (1991) should be satisfied.

In combined flows, the numerical resolution of the described equations requires an iterative method. This is due to the fact that the pressure term forcing the stationary current is dependent on the flow condition and on its vertical turbulence structure, which is *a priori* unknown. Assuming that mean current intensity, bed roughness, mean water depth, wave height and wave period are known parameters, the procedure to solve the problem is as follows:

1. In order to numerically solve the vertical structure of the pure current flow, a first run is performed. The run continues until a stationary condition is achieved, computing the pressure gradient needed to create this pure current flow.
2. After that, in a separate run, the wave–current combined flow structure is solved. The run starts with the initial condition derived from the output of the pure current case. The model is run until a stationary condition is achieved and a first guess of the mean velocity is obtained. If the estimated mean current velocity differs

from the one initially considered, the stationary part of the pressure gradient is modified according to the difference between the computed and the initially assumed mean current value. This procedure is repeated until the estimated mean velocity converges to the initially considered value. The numerical convergence in most of the wave–current runs considered in the present paper is satisfied within about 30 wave periods.

3. Model validation

In order to validate the developed model, previously published wave–current experimental data have been collected. The model has been applied to those conditions corresponding to each of the physical experiments. The numerically derived steady current profiles are compared with those measured in wave–current flumes and basins. During the validation process, the widest possible range of experimental conditions has been taken, considering those tests with waves opposing, following and perpendicular to currents. Most of the experimental tests were performed with monochromatic waves. Nevertheless, some irregular or spectral cases are also taken into account. The spectral cases are simulated with an equivalent monochromatic wave. This equivalent monochromatic wave is characterized by the root mean square wave height, H_{rms}, and by the peak period of the spectral wave, T_p. Note that the bed roughness in each of the tests is obtained applying a logarithmic fit to the pure current profile. This is usually measured before running the combined case.

This section is divided into three different parts according to the angle of propagation between waves and currents. First the validation of the following cases is shown, next the opposite ones and finally the perpendicular cases.

3.1. Following waves and currents

Table 1 indicates the characteristics of each of the considered tests: wave height, wave period, mean water depth, relative wave height, depth and wave period averaged current intensity, the physical bed roughness and wave type (monochromatic or spectral). In the spectral case H represents H_{rms} and T stands for Tp.

The experiments carried out by Kemp and Simons (1982) with following waves and currents over a smooth bottom showed that when increasing the wave height, the reduction of the current velocities in the upper part of the water column becomes more important. Moreover, the reduction in the upper part of the water column is followed by an increase near the bottom. Fig. 3 shows the comparisons of the model results with two different tests performed by Kemp and Simons (1982). In the same figure the logarithmic profile of a pure current characterized by the same intensity and affected by the same bed roughness has been depicted. The results showed that a good agreement between the computed and the measured profiles is achieved. It is worth pointing out that the model is able to predict the reduction of the current intensity just below the wave trough level and the intensification near the bottom. However, the agreement between the measurements and the computed profile

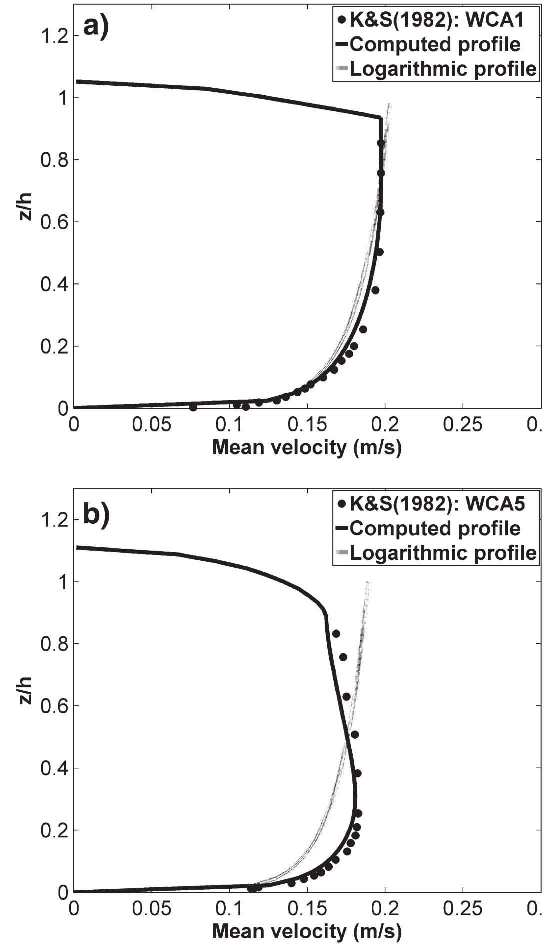

Fig. 3. Comparison between measured and predicted current profiles, (Kemp and Simons, 1982). a) WCA1, b) WCA5. Dotted lines represent the experimental measurements; continuous line represents the computed steady current profile; grey lines represent the profiles calculated by a logarithmic equation.

is less satisfactory in the test WCA5 than in WCA1. Both tests differ in the wave heights, being the test WCA5 the most non-linear case. It is important to point out that the present model takes into account the water level variation induced by the finite amplitude of the waves. However it considers sinusoidal waves. When waves are non-linear the wave shape is modified resulting in sharper wave crests and less pronounced wave troughs. This change in the wave form could affect the wave averaged currents vertical profiles as its result is an asymmetry on the wave orbital velocities.

The experiment by Klopman (1994) is the one with the minimum relative water depth considered in the present paper and represents one of the most non-linear cases. The measured mean profile confirmed the findings of Kemp and Simons (1982): below the wave crest, a reduction of the current velocity was observed with an increase near the bottom. Fig. 4 depicts the comparison between the computed velocity profile and the measured one. The obtained determination coefficient (defined in the Appendix A) is 94.1%. Although the model overestimates the increase of the current velocity near the bottom, a reasonable agreement between the computed and measured profiles is obtained. The discrepancies could be due to the simplicity of the vertical turbulence closure model, or due to processes that are not considered in the model, such as wave decay or the change in the wave shape from the sinusoidal form considered in the model. These changes in the wave shape are produced when waves are non linear waves.

Note that in the upper part of the water column the model predicts an important enhancement of the current speed. This region

Table 1
Laboratory test characteristics. K&S (1982) = Kemp and Simons (1982); K (1994) = Klopman (1994); U (2005) = Umeyama (2005); N&K (1987) = Nieuwjaar and Van der Kaaij (1987); Monochromatic = M; Spectral = S; Jonswap = J.

Test	H (cm)	T (s)	h (cm)	H/h	U (cm/s)	z_0 (m)	Type
K&S (1982) WCA1	2.07	1.0	20	0.1035	18.3	0.00001	M
K&S (1982) WCA5	4.44	1.0	20	0.222	18.3	0.00001	M
K (1994)	12	1.4	50	0.1	15	0.00037	M
U (2005) WCF1	1.75	0.9	20	0.0875	12	0.00003	M
U (2005) WCF4	2.5	1.4	20	0.125	12	0.00003	M
N&K (1987)	5.2	2.6	51.2	0.1	11.3	0.002	S (J)

Please cite this article as: Olabarrieta, M., et al., Effects of wave–current interaction on the current profile, Coast. Eng. (2010), doi:10.1016/j.coastaleng.2010.02.003

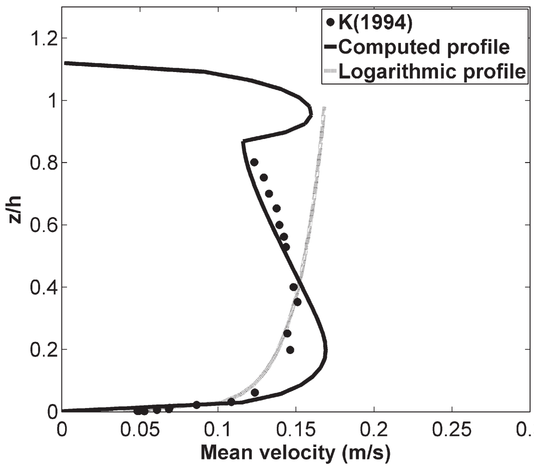

Fig. 4. Comparison between measured and predicted current profiles, (Klopman, 1994). Dotted lines represent the experimental measurements; the continuous line represents the computed steady current profile; grey line represents the profile calculated by a logarithmic equation.

corresponds to the zone between the wave trough and the crest. The observed flow increase occurs because during the wave propagation, this region does not always correspond to the water domain and, when it does, the water particles exhibit an orbital motion in the wave propagation direction. It is important to remark that without considering the α coordinate system transformation it is impossible to predict this Stokes Drift. In other words, if a rigid-lid approach is assumed for the free surface, the numerical model is not able to simulate this surface effect.

Umeyama (2005) analyzed the currents vertical structure based on the data measured in a wave–current flume, considering four different conditions for waves following the current. In these experiments not only the wave height was changed, but also the wave period. Measured profiles suggest that increasing the wave height, a more intense reduction of the velocity just below the wave trough occurs. This effect is followed by an increase of the flow near the bottom. However, as the wave period increases, the velocity reduction just below the wave trough is less important. Moreover, the near bottom velocity enhancement decreases. This fact suggests that the increase of the height can counteract the enhancement of the wave period. This can be justified by considering that the phase-averaged Reynolds stresses generated by waves represent the phase average correlation between the horizontal and the vertical particle motion. In intermediate waters as the wave height increases, so does this correlation. On the contrary, as the wave period increases, the vertical component of the particle motion decreases, generating a reduction of the Reynolds stresses. In the upper part of the water column, where the vertical velocities are maximums, the oscillatory motion vertical component is of great importance. This confirms, as suggested by Huang and Mei (2003), the existence of a surface boundary layer that affects the flow structure over the whole water column.

In Fig. 5 the comparison between computed profiles and those measured by Umeyama (2005) is shown. The first case (WCF1) is the most linear, while case (WCF4) corresponds to the most non-linear case. On the other hand, the wave period increases from WCF1 to WCF4.

In all the cases, a good agreement is achieved between the measured and computed profiles. However, for the WCF4 test a deviation is observed near the bed, where the numerical model underestimates the current velocity. This also occurs in the upper part of the water column where the model over predicts the current intensity. The main difference between these two experiments is the non-linearity. In the experiment WCF1, the ratio between the wave

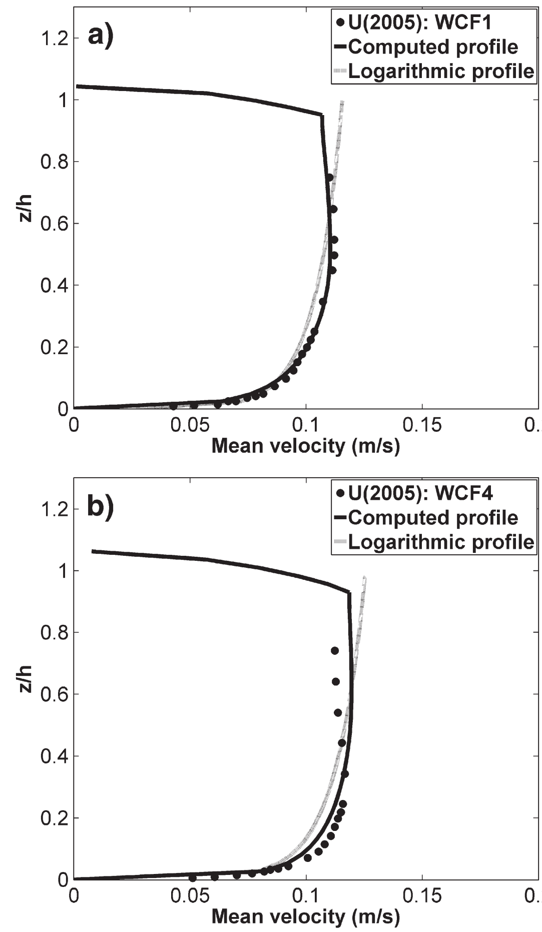

Fig. 5. Comparison between measured and predicted current profiles, (Umeyama, 2005). Dotted lines represent the experimental measurements; continuous lines represent the computed steady current profile; grey lines represent the profiles calculated by a logarithmic equation.

height and the water depth has a value of 0.08 while in WCF4 it increases to 0.125. The numerically reproduced wave averaged profile shows a good agreement with the measured profile in the WCF1 case, while for the WCF4 the results are less satisfactory. This could be created by the fact that in non-linear waves the wave form is not sinusoidal. Second or higher order Stokes waves would be more representative of this kind of waves. The asymmetrical shape characteristic of non-linear waves could create a change in the period average current profile, however other causes such as the non consideration of the wave dissipation could also be the cause of the observed differences.

Finally, the comparison for the spectral case corresponding to the experiments performed by Nieuwjaar and Van der Kaaij (1987) is shown in Fig. 6. As can be appreciated, although the flow is simulated with an equivalent wave height, a good estimation is obtained.

3.2. Opposing waves and currents

When waves propagate opposing the current, the effects on the mean current profile are very different compared to those obtained for the following ones. In order to verify whether the model is capable of predicting the effect of opposing waves or not, different experimental cases have been considered. In Table 2 the characteristics of each test are indicated.

Fig. 7 depicts the comparison between computed profiles and the measurements of Kemp and Simons (1983). Both tests are characterized by the same wave period but in WDR1 the wave height is smaller

Please cite this article as: Olabarrieta, M., et al., Effects of wave–current interaction on the current profile, Coast. Eng. (2010), doi:10.1016/j.coastaleng.2010.02.003

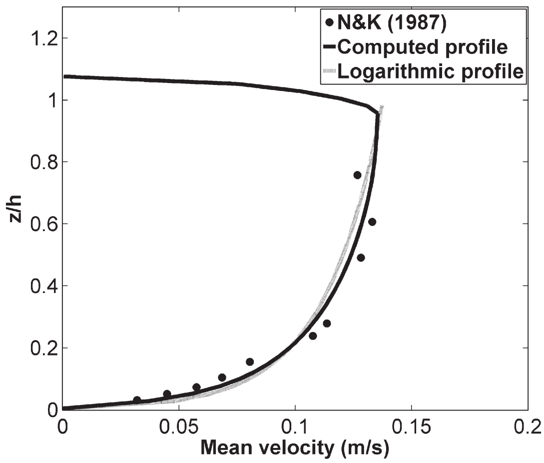

Fig. 6. Comparison between measured and predicted current profiles. Following case. Nieuwjaar and Van der Kaaij (1987). Dotted lines represent the experimental measurements; continuous line represents the computed steady current profile; grey line represents the profile calculated by a logarithmic equation.

than in WDR4. In opposition to what happens in the following cases, just above the wave trough level an increase of the current intensity is achieved. This enhancement is more pronounced as the wave height increases. As shown in the figure, the model underestimates the increase of the current speed just above waves trough level in the test WDR1. However, in the rest of the water column a good agreement is obtained. In the most non linear case (WDR4) the current profile is correctly reproduced by the numerical model.

In Figs. 8 and 9 the same comparison is made, but in these cases the tests carried out by Klopman (1994) and Umeyama (2005) are shown.

For the test performed by Klopman (1994) the numerical model slightly overestimates the mean current profile in the middle part of the water column. However, given the simplicity of the model, a reasonable agreement with the measurements is obtained. For the test of Umeyama (2005) a very good agreement is achieved. Contrarily to what was observed in the wave–current following cases, in the opposing ones a strong reduction of the current speed is observed in the upper part of the water column, that is, in the region between the wave crest and trough. In the opposing cases, the Stokes drift flows in the direction of wave propagation, in these cases, opposing to the current. That is the explanation of the observed reduction.

3.3. Perpendicular waves and currents

Finally, some comparisons for perpendicular cases are carried out. Table 3 indicates the characteristics of the considered tests, while in Figs. 10 and 11 the comparison between measured and computed current profiles is depicted.

In all the cases, a very good agreement between measured and computed profiles is obtained. Similarly to that which occurs in the opposing cases, a reduction of the current velocity is observed above the wave trough level in all the considered cases. The numerical

Table 2
Laboratory test characteristics. Opposing cases. K&S (1983) = Kemp and Simons (1983); U (2005) = Umeyama (2005); N&K (1987) = Nieuwjaar and Van der Kaaij (1987); Monochromatic = M; Spectral = S; Jonswap = J. 0.203.

Test	H (cm)	T (s)	h (cm)	H/h	U (cm/s)	z_0 (m)	Type
K&S (1983) WDR1	2.79	1.0	20	0.1395	18.3	0.0023	M
K&S (1983) WDR4	3.97	1.0	20	0.1985	18.3	0.0023	M
K (1994)	12	1.4	50	0.24	15	0.00037	M
U (2005) WCA1	1.8	0.9	20	0.09	12	0.00003	M
U (2005) WCA4	2.70	1.4	20	0.135	12	0.00003	M

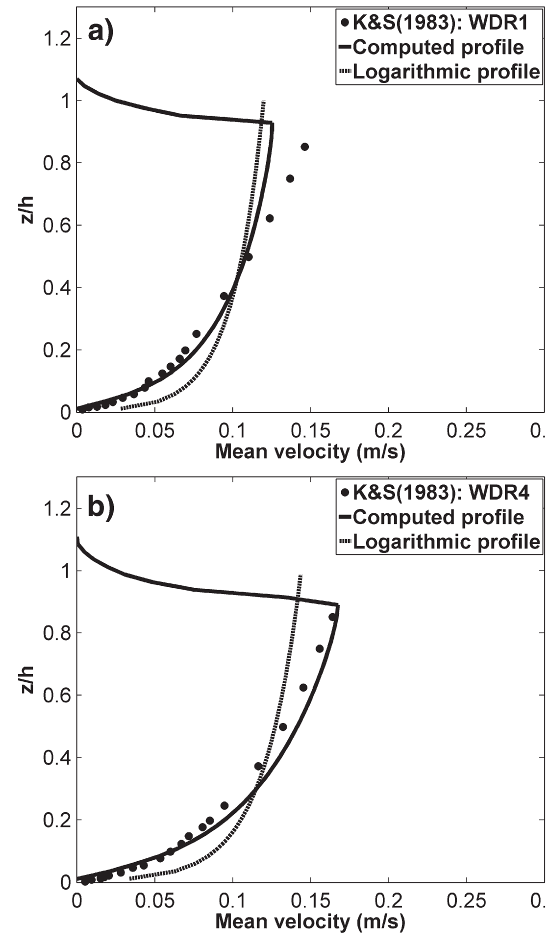

Fig. 7. Comparison between measured and predicted current profiles. a) Kemp and Simons (1983), WRD1; b) Kemp and Simons (1983), WRD4. Dotted lines represent the experimental measurements; continuous line represents the computed steady current profile; grey lines represent the profiles calculated by a logarithmic equation.

simulations of the experiments by Visser (1986) showed that in the test T241 the reduction of the velocity in the upper part of the water column is higher than in the test T441, mainly because the wave height is higher. This reduction of the velocity is compensated with a stronger current in the mid-lower part of the water column increasing

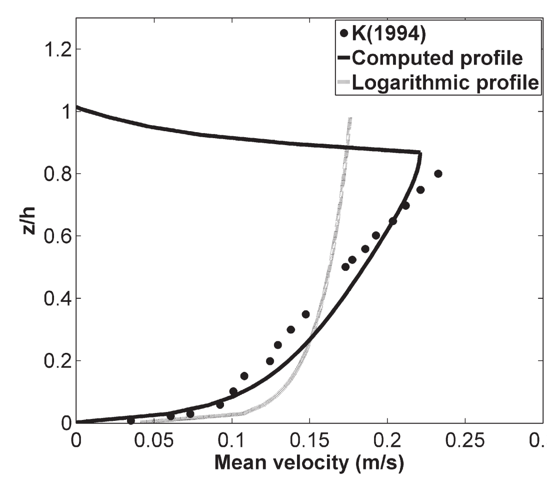

Fig. 8. Comparison between measured and predicted current profiles, Klopman (1994). Dotted lines represent the experimental measurements; the continuous line represents the computed steady current profile; grey line represents the profile calculated by a logarithmic equation.

Please cite this article as: Olabarrieta, M., et al., Effects of wave–current interaction on the current profile, Coast. Eng. (2010), doi:10.1016/j.coastaleng.2010.02.003

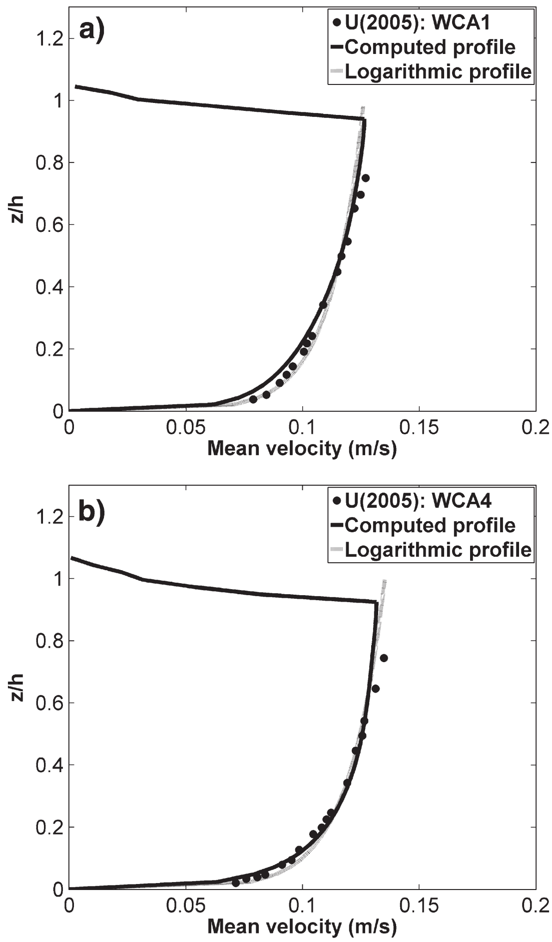

Fig. 9. Comparison between measured and predicted current profiles. a) Umeyama (2005), WCA1 b) Umeyama (2005), WCA4. Dotted lines represent the experimental measurements; a continuous line represents the computed steady current profile; grey lines represent the profiles calculated by a logarithmic equation.

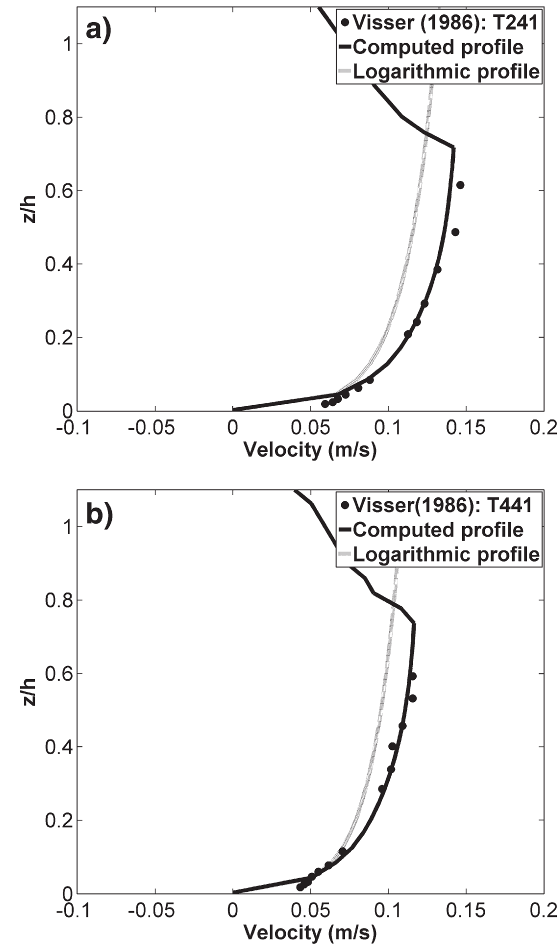

Fig. 10. Comparison between measured and predicted current profiles. a) Visser (1986), T241 b) Visser (1986), T441. Dotted lines represent the experimental measurements; the continuous line represents the computed steady current profile; grey lines represent the profiles calculated by a logarithmic equation.

the current shear. The same could be argued for the experiments by Musumeci et al. (2006). In the test case T14, the reduction of the current velocity was higher than in the experiment T08 and therefore the observed current shear in T14 in the mid- and bottom part of the water column is higher. Musumeci et al. (2006) suggested that in order to conserve mass in their experiments, the increase of the velocity in the lower part of the water column that was observed in most of their experiments should be balanced by an equivalent decrease of the velocity in the upper part. Simons et al. (1996) analyzed the vertical structure of the wave averaged profiles and the bottom shear stresses in orthogonal wave–current conditions. As shown in the Figure 6 of Simons et al. (1996) a reduction of the wave period averaged current velocity in the upper part of the water column was observed when waves were superimposed to the current. The present model does not assume a rigid lid condition for the free surface and therefore is able to simulate the reduction of the velocity in the upper part of the water column.

Table 3
Laboratory test characteristics. Perpendicular cases. V (1986) a = Visser_T241(1986); V (1986) b = Visser_T441 (1986); M (2006) a = Musumeci et al. (2006); M (2006) b = Musumeci et al. (2006); Monochromatic = M; Spectral = S; Jonswap = J.

Test	H (cm)	T (s)	h (cm)	H/h	U (cm/s)	z_0 (m)	Type
V (1986) a	10.6	2.0	20	0.53	10.5	0.00033	M
V (1986) b	6.8	2.0	20	0.34	10.5	0.00033	M
M (2006) a	8.5	1.4	30	0.28	4.4	0.00002	M
M (2006) b	8.5	0.8	30	0.28	4.4	0.00002	M

As it was mentioned in the introduction section, Huang and Mei (2003) attributed the change in the flow profile to a large distortion of the eddy viscosity at the free surface, while Groeneweg and Battjes (2003) concluded that it was due to the vorticity generation and wave decay, that produce a wave-induced imbalance in the shear stress. The present model does not include any wave decay and, even so, it is able to reproduce reasonably well the change in the current profile. Therefore, it can be concluded that the wave decay produces a smaller effect than the vorticity generation induced by the vertical variation of the oscillatory velocities.

4. Variation of the apparent bed roughness

One of the most important effects of wave–current interaction is the variation of the apparent bed roughness. If the steady current profile is known, the apparent bed roughness can be estimated by fitting a logarithmic profile. In the present paper a simple least-square method is applied to fit the following logarithmic profile:

$$U(z) = \left[\frac{U}{\frac{z_a}{h} - 1 + \ln\left(\frac{z_a}{h}\right)}\right] \ln\left(\frac{z}{z_a}\right) \tag{32}$$

Where z_a represents the elevation at which the logarithmic current profiles is null. The fitting is only performed along the logarithmic layer, obtaining the value of z_0 for the combined flow. Considering

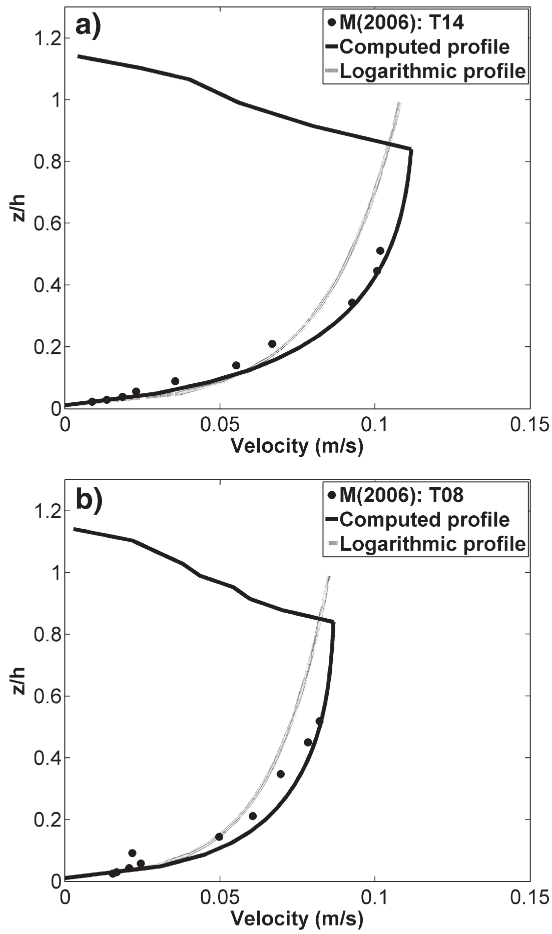

Fig. 11. Comparison between measured and predicted current profiles. a) Musumeci et al. (2006), T14 b) Musumeci et al. (2006), T08. Dotted lines represent the experimental measurements; a continuous line represents the computed steady current profile; grey lines represent the profiles calculated by a logarithmic equation.

that $k_s = 30z_0$ and $k_a = 30z_a$, the variation of the apparent bed roughness $\frac{k_a}{k_s}$ is equivalent to the relation $\frac{z_a}{z_0}$.

The fitting is only performed along the logarithmic layer. Following the aforementioned procedure, in all the experimental profiles considered in the validation process the zero velocity elevation z_a has been evaluated. This parameter has also been evaluated for pure current conditions. The same procedure has been followed with the computed profiles. Moreover, for each experimental condition the variation of the apparent bed roughness given by Grant and Madsen (1979), Fredsøe (1984) and Davies et al. (1988) has also been computed. These were derived from the approximate functions given by Soulsby et al. (1993), specified in the Appendix B. Note that none of these models considers the difference between opposing and following waves and currents.

In Fig. 12 the comparison of the measured and the computed increase of the apparent bed roughness is depicted. The figure is divided into four different panels: in the upper left hand panel, all the data has been plotted, covering all the possible angles between waves and currents. The other three panels represent the data separated in function of the ϕ angle. As it can be appreciated, for following wave current cases ($\phi = 0°$), all the models to the exception of the current model tend to overestimate the increase of the apparent bed roughness. This behaviour is especially significant in the case of Grant and Madsen (1979). Notice that there are three cases (corresponding to the experiments of Kemp and Simons, 1982 and Umeyama, 2005) in which a decrease of the apparent bed roughness occurs. All the models, with the exception of the one presented in the present paper, predict an increase instead of a decrease of this parameter. For the perpendicular and opposing cases, a better agreement between the different models and the measured data is observed. However, in the opposing cases the models of Grant and Madsen (1979), Fredsøe (1984) and Davies et al. (1988) tend to under predict the analyzed parameter. It is to point out that the experiment of Klopman (1994) with opposing waves and current generated an increase of the apparent bed roughness in two orders of magnitude. None of the models to the exception of the present one is able to predict the observed increase.

5. Changes in the current profile

This section is focused on the effects that the variation on the wave height and the wave period can create in the steady current profile. With that aim, different numerical runs have been performed. In the first set of runs all the parameters were maintained constant except the wave height. The considered water depth is 1 m, with a bed of small roughness ($z_0 = 0.01$ mm), the wave period corresponds to 4 s and the mean current intensity has been set to 0.1 m/s. The steady current profiles obtained by varying the wave height are shown in Fig. 13. For following waves and currents, in all the cases an important increase of the current velocity is observed above the wave trough level. This is caused due to the mass transport between the wave trough and crest. As the wave height increases, the mass transport in this upper layer also increases. Below this upper zone, a reduction of the current intensity, followed by an increase in the lower part of the water column is observed. As the wave height increases, the deviation from the logarithmic profile is more pronounced. For most energetic waves, an intensification of the current velocity near the bed is detected, corresponding to a decrease in the apparent bed roughness. The observed effects in the opposing waves and currents are contrary to those in the following cases. In opposing waves and currents, the mass transport in the upper part of the water column is opposing the current, creating a reduction of the current velocity. In most nonlinear opposing cases this superficial currents can show negative velocities. Counteracting this effect, in the middle part of the water column an increase of the current intensity is achieved.

In all the analyzed cases, the presence of waves creates an increase of the apparent bed roughness, reducing the current intensity near the bed. This reduction increases as the wave energy is enhanced.

Fig. 14 depicts the steady current profiles obtained for different wave periods. As the wave period increases, the mass transport in the upper layer does so also. In the following cases this transport is in the direction of the current, and in the opposing cases in the contrary direction. Below the trough level, an important reduction of the current velocity is observed especially for the small period cases if the waves are following the current. This is counteracted by an important increase of the current near the bottom, creating a reduction of the apparent bed roughness. If the waves are opposing the current, the variation on the wave period creates less important changes on the steady current profile. It can be seen that when the wave period decreases, the current becomes more intense below the wave trough level and the near bottom velocity is also reduced. However, the observed changes in the current profile are not that significant.

From the experimental data and the profiles obtained by numerical computation, three different regions can by distinguished on a current profile in a combined flow. The first one corresponds to the upper region, in which the flow is governed by the mass transport due to waves. The second part corresponds to the region below the wave trough, where wave induced Reynolds stresses generate a variation on the current profile. For following waves and currents, they generate a reduction of the current intensity, while for the opposing cases, an intensification is obtained. These changes on the current profile are more pronounced for high wave conditions. The last region corresponds to the near bottom region. In general, a reduction of the current intensity due to the enhancement of the

Please cite this article as: Olabarrieta, M., et al., Effects of wave–current interaction on the current profile, Coast. Eng. (2010), doi:10.1016/j.coastaleng.2010.02.003

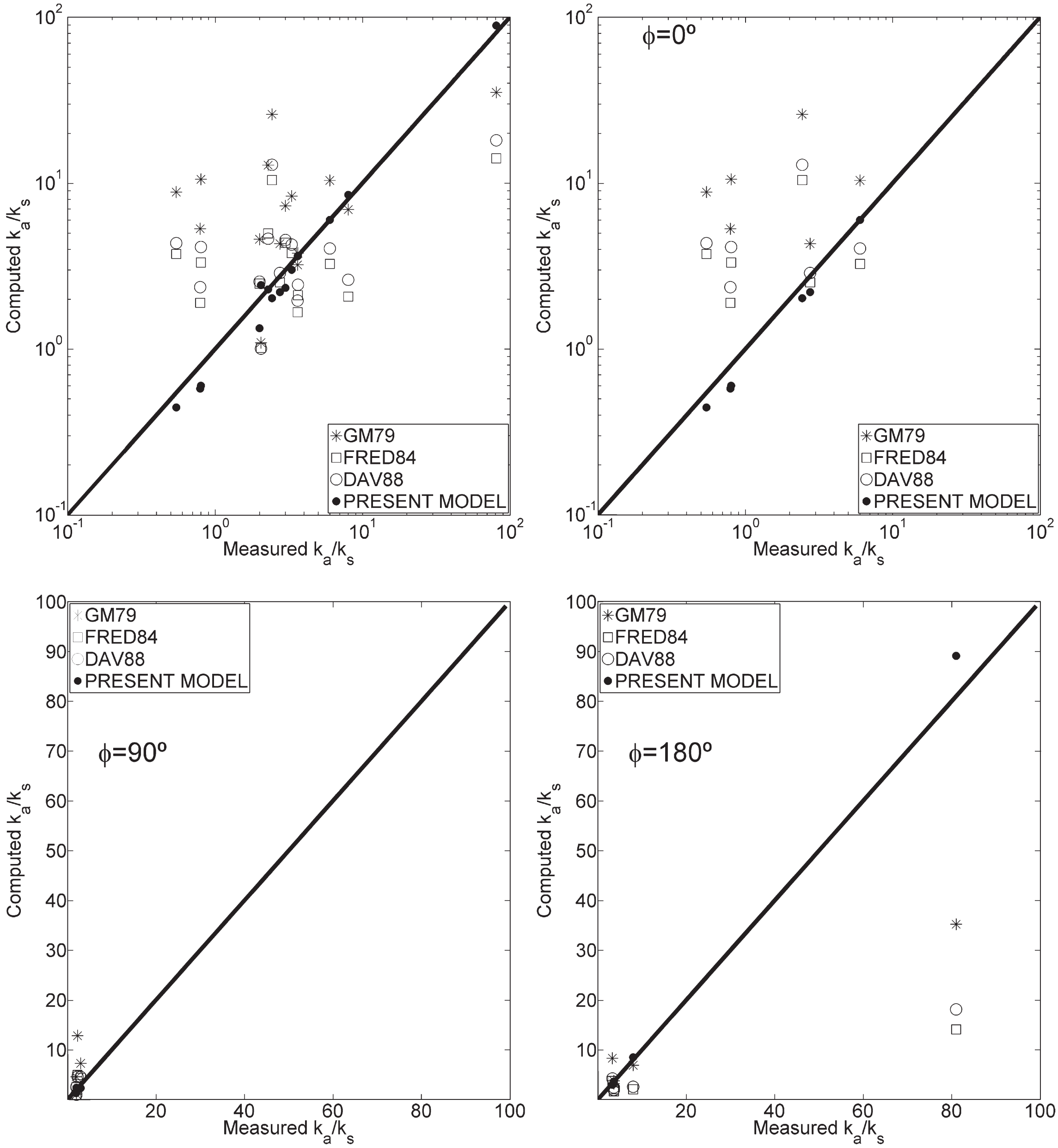

Fig. 12. Computed versus measured increase of the apparent bed roughness for the experimental conditions considered in the model validation considering following, opposing and perpendicular wave current conditions. The stars represent the prediction of Grant and Madsen (1979) versus the measured data, the squares represent the results given by Fredsøe (1984) versus the measured data, the circles represent the results given by the model of Davies et al. (1988) compared to the measured data and the dots represent the present model estimations compared to the measured data.

apparent bed roughness is observed in this region. However, there are several cases for following conditions in which wave–current interaction produces a reduction of the apparent bed roughness. Therefore the current intensity in this zone increases. This unexpected reduction of the apparent bed roughness, due to the presence of waves, has been observed in experimental data (Klopman, 1994, 1997) and Kemp and Simons (1982) and is now also observed through numerical modeling. These authors attributed the decrease of the apparent bed roughness to a different behaviour of the laminar wave boundary layers. They suggested that in laminar boundary flows, the addition of the wave induced currents to the steady current produces an increase of the flow near the bottom. However, in turbulent flows, the increase of turbulence induced by the oscillatory motion results in a reduction of the current intensity. In our opinion there are two possible processes contributing to this reduction. The first process is the wave streaming. The streaming is a residual current generated in the wave boundary layer that is caused by the spatial variations of the wave boundary layer thickness. The streaming flows in the direction of the wave propagation and therefore, in following wave–current conditions it could counteract the effects of the turbulence enhancement that is achieved in the near bed region. If the intensity of the streaming is high, it could create an increase the current velocity in the near bed region. On the other hand, for opposing wave–current flows the effect of the streaming is the same as the effect of the turbulence enhancement produced by the oscillatory motion, producing a further increase of the apparent bed roughness. Since the streaming can only be modelled by solving the spatial variation of the wave boundary layer thickness, it is necessary to at least solve the flow structure along a wave-length. The models of Grant and Madsen (1979), Fredsøe (1984) and Davies et al. (1988) are 1DV models, and thus are not able to reproduce this effect or the difference between opposing and following currents. The second

Please cite this article as: Olabarrieta, M., et al., Effects of wave–current interaction on the current profile, Coast. Eng. (2010), doi:10.1016/j.coastaleng.2010.02.003

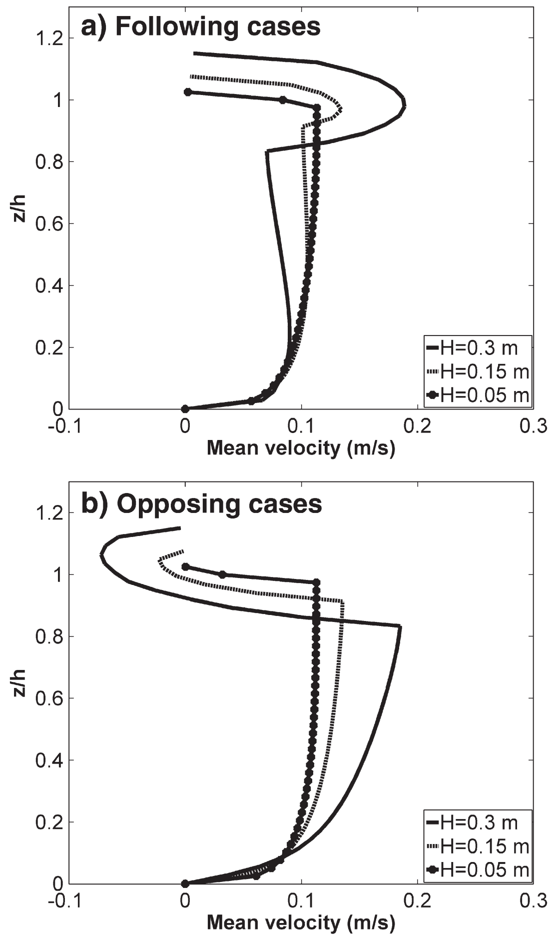

Fig. 13. Effect of the wave height variation on the vertical current profile for different angles between waves and currents. a) Following cases: $z_o = 0.01$ mm, $T = 4.$ s, $U = 0.1$ m/s. b) Opposing cases: $z_o = 0.01$ mm, $T = 4.$ s, $U = 0.1$ m/s. Continuous line represents the case in which $H = 0.3$ m, the discontinuous line represents the case with $H = 0.15$ m and the dotted line the case in which $H = 0.05$ m.

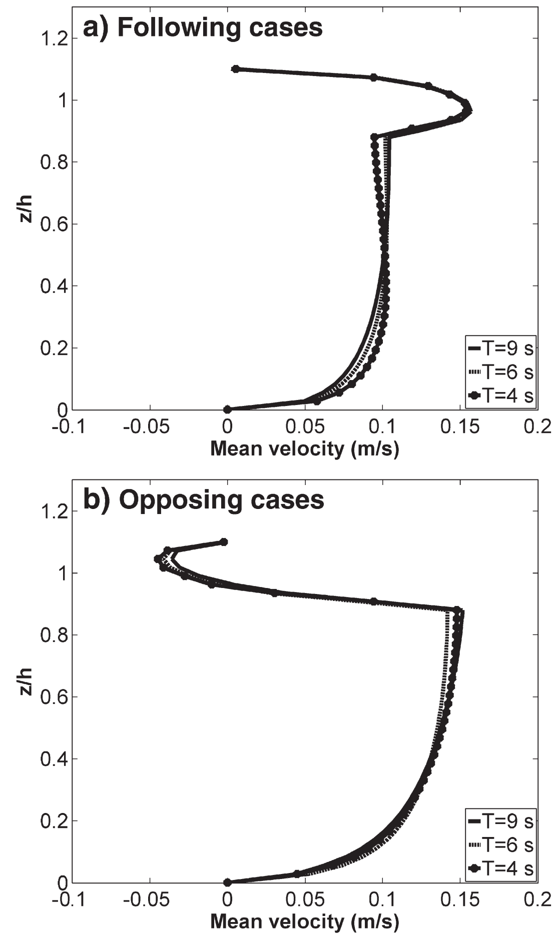

Fig. 14. Effect of the variation of wave period on the vertical current profile for different angles between waves and currents. a) Following cases: $z_o = 0.01$ mm, $H = 0.2$ m, $U = 0.1$ m/s. b) Opposing cases: $z_o = 0.01$ mm, $H = 0.2$ m, $U = 0.1$ m/s. Continuous line represents the case in which $T = 9$ s, the discontinuous line represents the case with $T = 6$ s and the dotted line the case in which $T = 4$ s.

process that could be creating the decrease of the apparent bed roughness is the compensation of the current reduction in the upper part of the water column. In order to compensate this decrease, an acceleration of the flow is achieved in the near bed region. This process is of special relevance in the perpendicular wave–current flows, but could also be relevant in the following cases.

6. Conclusions

A 2DV non hydrostatic model has been developed in order to analyze the effects of wave–current interaction on the mean steady currents profile. The model can simulate currents propagating at different angles with respect to the wave propagation direction, simulating following, opposing and oblique waves. In this model, the governing equations are solved in the classical Eulerian reference frame, but using an α vertical coordinate system. This enables us to introduce the free surface elevation variation due to the oscillatory motion, without assuming the rigid-lid approach.

The model has been tested with vertical steady current profiles measured from different laboratory experiments. These cover different conditions in which the wave–current interaction can take place with following, opposing, and perpendicular wave–current flows. Experiments considering monochromatic and spectral waves have been used in the validation process. The comparison between measured and computed current profiles has evidenced that the model is able to accurately solve the vertical structure of the combined flows for all the values of the ϕ angle as well as for the considered current regimes. Moreover, when the spectral cases are simulated with an equivalent monochromatic wave, characterized by the peak period and the root mean square wave height, the computed profiles are very similar to the measured ones.

The model has been used to analyze the effect of wave height and wave period on the steady current profile for opposing and following wave–current conditions. Starting from the angle ϕ, there is a big difference between those profiles obtained for following and opposing currents. Between the wave crest and trough level, an increase of the flow is achieved for the following cases, while a decrease characterizes the opposing ones. This is caused by the Stokes drift, known as the wave induced mass flux in the direction of wave propagation. In the perpendicular cases, a reduction of the flow velocity is observed. This is compensated with an intensification in the lower part of the water column, as observed by Musumeci et al. (2006). Below the wave trough level, the differences for different angles between waves and currents are still apparent. While for the following cases a reduction of the velocity is observed just below the wave trough level, intensification occurs in the opposing ones. These changes become more evident as the wave height increases and as the wave period decreases. For intermediate water depths, an important reduction of the flow is observed for following waves and currents due to the effect of the Reynolds stresses.

It is also important to point out that the effect of wave–current interaction is not restricted only to the bottom wave boundary layer region but to the entire water column. Usually, the effect of waves on currents is introduced by an increase of the apparent bed roughness, which in most of the cases is not dependent on the ϕ angle. Moreover, as shown by the experimental data, the present work has corroborated what was shown by previous authors regarding the decrease of the apparent bed roughness in following wave–current conditions. The present study has shown that in some wave–current conditions characterized by small bed roughness, energetic waves propagating in intermediate waters create an important flow reduction just below the wave trough level due to the effect of the Reynolds stresses. In these cases the flow resistance in the bottom wave boundary layer is smaller than the resistance in the upper part of the water column and thus the flow tends to accelerate in the region near the bed.

The present work has evidenced the need of considering the propagation angle between waves and currents when modeling the hydrodynamics and sediment transport in combined flows, because the effects in both cases are completely different. However, most of the *two step* models applied nowadays to combine flows do not consider this difference. Therefore, in order to correctly model the wave current interaction through "two-step" hydrodynamic models, it is necessary to include somehow the effect of the vertical Reynolds stresses induced by the wave motion. Extension of this study to derive the corresponding closure models for the Reynolds stresses and to determine the apparent bed roughness considering the angle between waves and currents is underway.

Acknowledgements

This publication was developed inside the framework of the research project CTM 2008-06640/MAR (Modelado de la evolución morfodinámica de playas en medio plazo) by the Spanish Ministry of Innovation and Science and it also has been partly funded by the Spanish Ministry of Education and Science under the research project TRA2007-65133/TMAR (PREVER project). The anonymous reviewers are thanked for their comments and suggestions.

Appendix A

The coherence between the model and measurements was analyzed by the determination coefficient (R^2). Considering that M_n and C_n are the measured data and the computed data respectably at N discrete points, the determination coefficient (R^2) between M_n and C_n is defined by:

$$R^2 = \left(\frac{\frac{1}{N} \sum_{n=1}^{N} \left(M_n - \overline{M_n}\right)\left(C_n - \overline{C_n}\right)}{\sigma_C \sigma_M} \right)^2 \tag{A.1}$$

where σ_M and σ_C are the standard deviations of the measured and computed data respectively.

Appendix B

Soulsby et al. (1993) derived an algebraic approximation (accurate to $\pm 5\%$ in most cases) for some of the boundary layer models available in the state of art to compute the bottom shear stress in wave–current combined flows. The total bed shear stress over a wave cycle, for a sinusoidal wave is given by the following expression:

$$\tau_{m,wc} = Y(\tau_c + \tau_w) \tag{B.1}$$

where $\tau_{m,wc}$ is the total mean shear stress, τ_c is the bottom shear stress in pure current conditions and τ_w represents the bed shear in pure wave conditions. Y is defined by the following expression:

$$Y = X\left[1 + bX^p(1-X)^q\right] \tag{B.2}$$

where

$$b = \left(b_1 + b_2|\cos\phi|^j\right) + \left(b_3 + b_4|\cos\phi|^j\right)\log_{10}\left(\frac{f_w}{C_D}\right) \tag{B.3}$$

$$p = \left(p_1 + p_2|\cos\phi|^j\right) + \left(p_3 + p_4|\cos\phi|^j\right)\log_{10}\left(\frac{f_w}{C_D}\right) \tag{B.4}$$

$$q = \left(q_1 + q_2|\cos\phi|^j\right) + \left(q_3 + q_4|\cos\phi|^j\right)\log_{10}\left(\frac{f_w}{C_D}\right) \tag{B.5}$$

The values of the coefficients for the formulations of Grant and Madsen (1979) (GM79), Fredsøe (1984) (F84) and Davies et al. (1988) (DKS88) are presented in Table B1:

With the wave friction factor defined as (Soulsby et al., 1993):

$$f_w = 1.39\left(\frac{A}{z_0}\right)^{-0.52} \tag{B.6}$$

where A stands for the semi-orbital excursion. The current drag coefficient C_D is defined as:

$$C_D = \left[\frac{0.4}{1 + \ln\left({}^{z_0}/_{h}\right)}\right]^2 \tag{B.7}$$

The total mean bottom shear stress can also be expressed as:

$$\tau_{m,wc} = \rho C_{D,wc} U^2 \tag{B.8}$$

where $C_{D,wc}$ represents the drag coefficient under wave–current conditions and is related with the apparent physical bed roughness by the following relation:

$$C_{D,wc} = \left[\frac{0.4}{1 + \ln\left({}^{z_a}/_{h}\right)}\right]^2 \tag{B.9}$$

References

Bakker, W.T., Van Doorn, T., 1978. Near bottom velocities in waves with a current. Proceedings of 16th International Conference on Coastal Engineering, Hamburg, pp. 1394–1413.

Bolaños-Sanchez, R., Riethmüller, R., Gayer, G.L.C., Amos, 2005. Sediment transport in a tidal lagoon subject to varying winds evaluated with a coupled current-wave model. Journal of Coastal Research 21 (2), e11–e26.

Christoffersen, J.B., Jonsson, I.G., 1985. Bed friction and dissipation in a combined current and wave motion. Ocean Engineering 12, 387–423.

Davies, A.G., Soulsby, R.L., King, H.L., 1988. A numerical model of the combined wave and current bottom boundary layer. Journal of Geophysical Research 93 (C1), 491–508.

Table B1
Fitting coefficients for wave/current boundary layer models.

	b1	b2	b3	b4	p1	p2	p3	p4	q1	q2	q3	q4	J
GM79	0.73	0.4	−0.23	−0.24	−0.68	0.13	0.24	−0.07	1.04	−0.56	0.34	−0.27	0.5
F84	0.29	0.55	−0.1	−0.14	−0.77	0.1	0.27	0.14	0.91	0.25	0.5	0.45	3.0
DSK88	0.22	0.73	−0.05	−0.35	−0.86	0.26	0.34	−0.07	−0.89	2.33	2.60	−2.50	2.7

Dingemans, M.W., Van Kester, J.A.Th.M., Radder, A.C., Uittenbogaard, R.E., 1996. The effect of CL-vortez force in 3D wave–current interaction. Coastal Engineering: Proc. 25th Intl Conf. ASCE, pp. 4821–4832.

Fredsøe, J., 1984. Turbulent boundary layer in wave–current motion. Journal of Hydraulic Engineering, ASCE 110, 1103–1120.

Grant, W.D., Madsen, O.S., 1979. Combined wave and current interaction with a rough bottom. Journal of Geophysical Research 84 (C4), 1797–1808.

Groeneweg, J., Battjes, J., 2003. Three-dimensional wave effects on a steady current. Journal of Fluid Mechanics 478, 325–343.

Groeneweg, J., Klopman, G., 1998. Changes of the mean velocity profiles in the combined wave–current motion in a GLM formulation. Journal of Fluid Mechanics 370, 271–296.

Haney, R., 1991. On the pressure gradient force over steep topography in sigma coordinate ocean models. Journal of Physical Oceanography 21, 610–619.

Harris, J., 1997. Modelling random wave boundary layer flows. PhD thesis, University of Liverpool, Liverpool, U.K.

Holmedal, L.E., Myrhaug, D., Rue, H., 2003. The sea bed boundary layer under random waves plus current. Continental Shelf Research 23 (7), 717–750.

Huang, Z., Mei, C.C., 2003. Effects of surface waves on a turbulent current over a smooth or rough seabed. Journal of Fluid Mechanics 497, 253–287.

Huynh-Thanh, S., Temperville, A., 1991. A numerical model of the rough turbulent boundary layer in combined wave and current interaction. In: Soulsby, R.L., Bettess, R. (Eds.), Sand transport in Rivers, Estuaries and the Sea. Balkema, Rotterdam, pp. 93–100.

Kajiura, K.A., 1968. A model for the bottom boundary layer in water waves. Bulletin Earthquake Research 45, 75–123.

Kang, K., Iorio, D., 2006. Depth- and current-induced effects on wave propagation into the Altamaha River Estuary, Georgia. Estuarine, Coastal and Shelf Science 66, 395–408.

Kemp, P.H., Simons, R.R., 1982. The interaction between waves and a turbulent current: waves propagating with the current. Journal of Fluid Mechanics 116, 227–250.

Kemp, P.H., Simons, R.R., 1983. The interaction of waves and a turbulent current: waves propagating against the current. Journal of Fluid Mechanics 130, 73–89.

Kim, H., O'Connor, B.A., Park, I., Lee, Y., 2001. Modeling the effect of intersection angle on near bed flows for waves and currents. Journal of Waterway, Port, Coastal and Ocean Engineering 127, 308–318.

Klopman, G., 1994. Vertical structure of the flow due to waves and currents. Progress report H840.30, Part II. Delft Hydraulics.

Klopman, G., 1997. Secondary circulation of the flow due to waves and current: laser-Doppler flow measurements for waves following and opposing a current. Tech. Rep. Delft Hydraulics Z2249.

Moon, I.J., 2005. Impact of a coupled ocean wave-tide-circulation system on coastal modeling. Ocean Modeling 8, 203–236.

Musumeci, R.E., Cavallo, L., Foti, E., Scandura, P., 2006. Waves plus currents crossing at a right angle: experimental investigation. Journal of Geophysical Research 111, C07019.

Myrhaug, D., Slaattelid, O.H., 1990. A rational approach to wave–current friction coefficients for rough, smooth and transitional turbulent flow. Coastal Engineering 14, 265–293.

Nezu, I., Rodi, W., 1986. Open-channel flow measurements with a laser Doppler anemometer. Journal of Hydraulic Engineering 112 (5), 335–355.

Nielsen, P., 1986. Suspended sediment concentrations under waves. Coastal Engineering 10, 23–31.

Nielsen, P., You, Z., 1996. Eulerian mean velocity under non-breaking waves on horizontal bottom. In: Edge, L. (Ed.), 25th International Conference on Coastal Engineering. Orlando, Florida, vol. 1, pp. 4066–4078.

Nieuwjaar, M., Van der Kaaij, T., 1987. Sediment transport in irregular non-breaking waves. Coastal Engineering Department, Delft University of Technology, Delft, The Netherlands.

O´Connor, B.A., Yoo, D., 1988. Mean bed friction of combined wave/current flow. Coastal Engineering 12, 1–21.

Sheng, Y.P., 1983. Mathematical modeling of three-dimensional coastal currents and sediment dispersion: model development and application. Technical Report 83-2, US Army Engineer Waterways Experiment Station, Vicksburg, Miss.

Simons, R., MacIver, R.D., Saleh, W.M., 1996. Kinematics and shear stresses from combined waves and longshore currents in the UK coastal research facility. Proceedings of the Coastal Engineering Conference, pp. 3481–3494.

Soulsby, R.L., Hamm, L., Klopman, G., Myrhaug, D., Simons, R.R., Thomas, G.P., 1993. Wave–current interaction within and outside the bottom boundary layer. Coastal Engineering 21, 41–69.

Uittenbogaard, R.E., 2000. 1DV Simulation of wave–current interaction. In: Edge, L. (Ed.), 27th International Conference on Coastal Engineering, Sydney, Australia, vol. 1, pp. 255–268.

Umeyama, M., 2005. Reynolds stresses and velocity distributions in a wave–current coexisting environment. Journal of Waterway, Port, Coastal and Ocean Engineering 131 (5), 203–212.

Visser, P.J., 1986. Wave basin experiments on bottom friction due to currents and waves. Proceedings of the 20th International Conference on Costal Engineering, Taipeh, Taiwan.

Please cite this article as: Olabarrieta, M., et al., Effects of wave–current interaction on the current profile, Coast. Eng. (2010), doi:10.1016/j.coastaleng.2010.02.003